COMMUNICATIONS MATERIALS

ARTICLE

https://doi.org/10.1038/s43246-020-0019-0 OPEN

Understanding degradation of organic light-emitting diodes from magnetic field effects

Masaki Tanaka [1], Ryo Nagata[1], Hajime Nakanotani[1,2]✉ & Chihaya Adachi [1,2]✉

The impact of magnetic field effects on the electroluminescence of organic light-emitting diodes is commonly used to characterize exciton dynamics such as generation, annihilation, and performance degradation. However, interpreting these effects is challenging. Here, we show that magnetic field effects in organic light-emitting diodes can be understood in terms of the magnetic response of device characteristics derived from polaron-pair and triplet exciton quenching processes, such as triplet-polaron interactions and triplet-triplet annihilation. Device degradation shows a clear relationship with the amplitude of the magnetic field effects, enabling non-destructive measurement of the degradation. The results and proposed mechanism provide a better understanding of magnetic field effects on organic light-emitting diodes and device degradation phenomena.

[1] Center for Organic Photonics and Electronics Research (OPERA), Kyushu University, 744 Motooka, Nishi, Fukuoka 819-0395, Japan. [2] International Institute for Carbon Neutral Energy Research (WPI-I^{2}CNER), Kyushu University, 744 Motooka, Nishi, Fukuoka 819-0395, Japan. ✉email: nakanotani@cstf.kyushu-u.ac.jp; adachi@cstf.kyushu-u.ac.jp

An internal electroluminescence quantum efficiency of nearly 100% can be achieved in organic light-emitting diodes (OLEDs) especially by utilization of phosphorescence and thermally activated delayed fluorescence (TADF) that involve intersystem crossing between the lowest excited singlet and triplet states (S_1 and T_1). However, a significant improvement in OLED stability is of crucial importance, particularly in blue OLEDs, so that they can be used in high-performance displays and light sources. To improve OLED lifetimes, a detailed understanding of degradation processes is required. Several mechanisms have been proposed[1–9]. For example, Kondakov et al. reported that chemical decomposition of the organic materials is a critical degradation route[1–4] that originates from high-energy particles, such as highly excited triplet excitons (T_n) and polarons (P^*), generated via triplet–triplet annihilation (TTA) or triplet–polaron annihilation (TPA)[5–8]

$$T + T \rightarrow S_0 + T_n\,(\mathrm{TTA}),$$

$$T + P \rightarrow S_0 + P^*\,(\mathrm{TPA}),$$

where T, P, and S_0 are a triplet exciton, a polaron, and the ground state. T_n and P^* have high enough energy to decompose organic molecules and generate exciton quenchers and carrier traps. Recently, we clarified that TPA was identified as being responsible for the degradation mechanism for TADF-OLEDs, and the generation of carrier traps, the change in carrier balance, and successive exciton deactivation during device aging that significantly affect OLED lifetimes[9]. It has been strongly suggested that the dynamics of triplet excitons is largely responsible for device degradation. However, no direct evidence has been presented, and a detailed analysis of exciton dynamics via nondestructive measurements is complex.

To probe the dynamics of excited triplet states, external magnetic fields are used to lift the degeneracy. Magnetic field effects on the electroluminescence properties of OLEDs were first reported in 2003 by Kalinowski et al.[10], where the field modulated the ratio of the singlet/triplet exciton yield. This was the result of modulating the ratio of singlet and triplet polaron pairs (^{1}PP and ^{3}PP). Numerous studies regarding the mechanism of magnetic field effects on OLEDs based on fluorescent[11,12], phosphorescent[13], exciplex[14], and TADF emitters[15,16] were investigated to unveil the underlying dynamics of exciton generation, radiation, and annihilation processes. PP[11,17], triplet–polaron interactions (TPI)[16,18], and TTA mechanisms[12,16] were mainly used to explain magnetic field effects. However, the interpretation of these effects has been unclear, and the relationship between exciton dynamics and OLED degradation has been lacking.

Here, we demonstrate that magnetic-field-modulated electroluminescence (magneto-electroluminescence, MEL) can be used to track triplet exciton dynamics in OLEDs during degradation. MEL signals from TADF-OLEDs were divided into low-field and high-field effects that corresponded to PP and TPI mechanisms, respectively. We also find that the high-field effects exhibit a clear dependence on the delayed fluorescence lifetimes (τ_ds) of TADF emitters. Based on the assignment of the origin of the MEL signals, we analyze those signals of degraded OLEDs that exhibited large amplitudes relative to those of pristine (undegraded) OLEDs. Then, we confirm that the shapes of the MEL profiles changed due to an exciplex formation according to the unwanted change in location of the carrier recombination zone. We thus nondestructively reveal exciplex formation at the interface between emission and hole-blocking layers that results in a low electroluminescence quantum yield.

Results and discussion

Assessment of magnetic field effects in various TADF-OLEDs. We focused on TADF emitter-based OLEDs (Fig. 1a). The complete device architecture is provided in Supplementary Fig. 1. First, the MEL profiles of undegraded OLEDs were analyzed to probe the origin of magnetic responses. Figure 1b shows typical MEL profiles of 4CzIPN-based OLED under constant-current condition (MEL_J). To assess the origin of the MEL profiles, we performed a fitting analysis based on the Lorentzian and non-Lorentzian equations[16–19]

$$\begin{aligned}\text{Magnetic field effect} &= (\text{Low} - \text{field effect}) + (\text{high} - \text{field effect})\\ &= \frac{A_L B^2}{B^2 + B_L^2} + \frac{A_H B^2}{(B + B_H)^2}\end{aligned} \quad (1)$$

where A_L and A_H are the amplitudes and B_L and B_H are the characteristic magnetic fields for low-field and high-field effects, respectively. The results are summarized in Fig. 1b and Table 1. The MEL profiles had two parts, indicating that there are two different mechanisms.

Because B_L is a comparable value for the PP mechanism, i.e., ~5 mT[16–19], the low-field effect originates from the PP mechanism that increases "bright" singlet excitons. The magnetic field suppresses the intersystem crossing between ^{1}PP and ^{3}PP states. In contrast, B_H was large (~100 mT). We compared it with the zero-field splitting values, i.e., D and E, of the excited triplet state of 4CzIPN reported previously[20,21], and good agreement suggested that the high-field effect results from the reaction of triplet excitons. The τ_ds of TADF emitters affect the MEL profiles, as shown in Fig. 1c. Although the signs of all the MEL_J profiles were positive, their shape and magnitude, especially in the high-field region, depended on the τ_ds. This behavior could be understood from the probability of triplet exciton reactions such as TTA and TPI that should strongly depend on τ_ds[22–24]. In fact, devices based on TADF emitters exhibiting long τ_d, such as 2CzPN, PIC-TRZ, and 3CzTRZ, showed steep rolloffs in electroluminescence efficiency, as shown in Supplementary Fig. 2.

Magneto-photoluminescence measurements confirmed that 20 wt% 4CzIPN:mCBP and 2CzPN:mCBP films did not exhibit clear magnetic responses in high magnetic fields (Supplementary Fig. 3). Thus, the contribution of a TTA event to the MEL_J can be negligible. Furthermore, no magneto-photoluminescence response suggests that PPs are not induced from excitons generated under photoexcitation, as introduced in phosphorescent emitter and host systems[25].

Considering the effect of TPI on MEL_J, Fig. 1d is a schematic of a TPI process in OLEDs under electrical excitation. A triplet–polaron (trion) intermediate state is formed when a triplet exciton and a polaron collide, and has two possible spin states: "doublet" and "quartet"[18,19,26]. Because the doublet-trion reaction, i.e., TPA, is spin-allowed, the T_1 that contributes to the reverse intersystem crossing (RISC) in TADF-OLEDs can be immediately quenched via energy transfer to the polaron, generating a ground-state molecule and an excited (hot) polaron. Because the energy of the hot polaron is enough high to dissociate chemical bonds, the TPA generates decomposed materials that are exciton quenchers and/or carrier traps. In contrast, the quartet state reaction is spin-forbidden and the lifetime of a quartet-trion is longer than that of the doublet. Thus, there are two possible quartet–trion reactions: "carrier scattering" and "exciton dissociation." In carrier scattering, a quartet–trion separates into a triplet exciton and a polaron, and the net charge carrier mobility is decreased. In contrast, the dissociation process increases the net carrier density because the triplet exciton dissociates into a hole and an electron via the quartet–trion

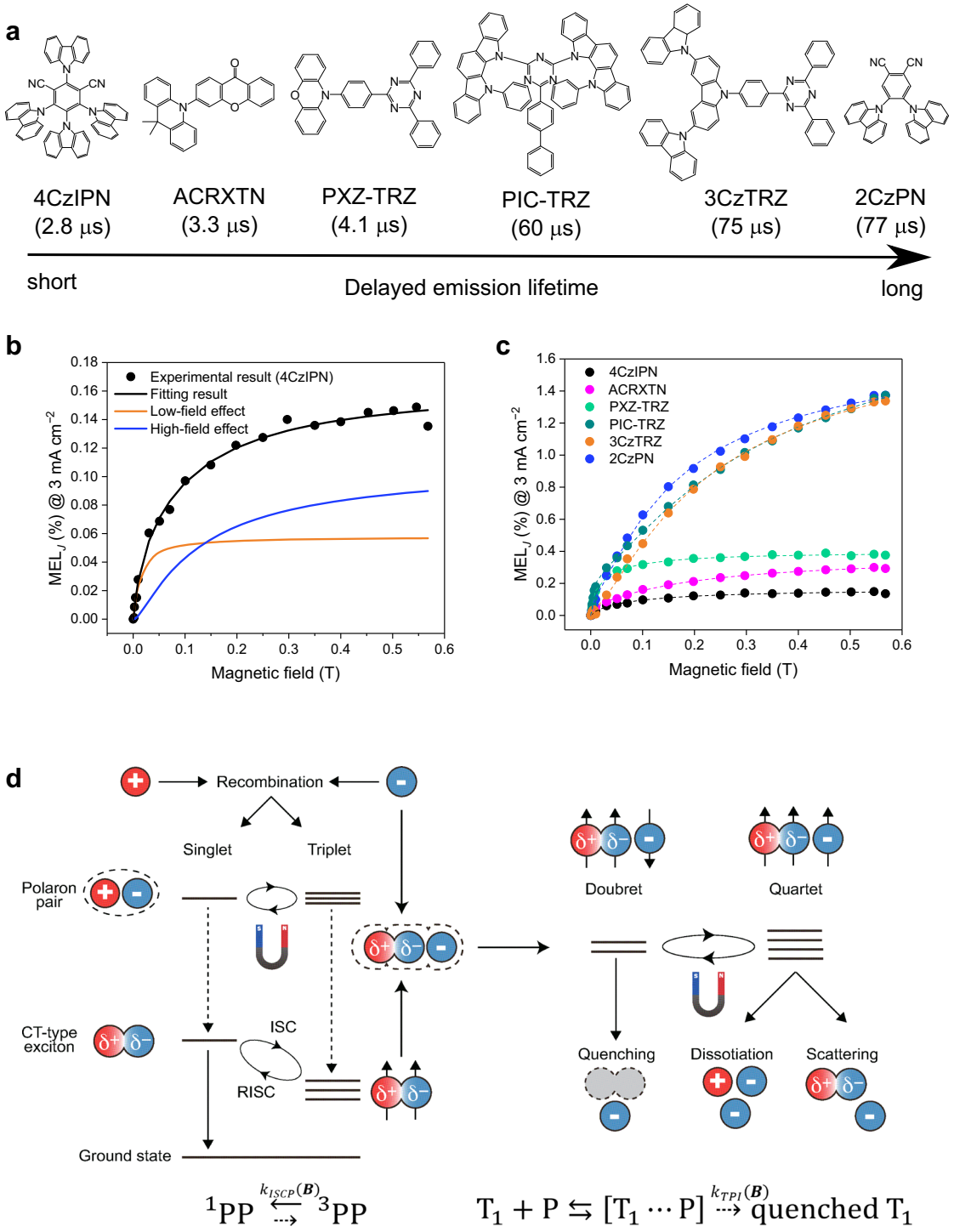

Fig. 1 Magnetic field effects on electroluminescence intensity of TADF-OLEDs. a Molecular structures of TADF emitters with delayed emission lifetimes. **b** Fit of magneto-electroluminescence profile of 4CzIPN-based OLED under constant 3.0 mA cm^{-2} current into low-field and high-field effects. **c** Magneto-electroluminescence profiles of various TADF-OLEDs. The dashed lines are fits. **d** Schematic of triplet-polaron interaction (TPI) in OLEDs under electrical excitation. A magnetic field suppresses the intersystem crossing of the polaron-pair state (small intersystem crossing rate, k_{ISCP}) and the triplet-polaron interaction (small triplet polaron interaction rate, k_{TPI}). [T_1···P] represents a trion intermediate state.

intermediate state. A magnetic field can suppress the interaction probability between a triplet exciton and a polaron, reducing the rates of TPA, scattering, and dissociation[17,18,23,26–28]. Hence, the emission and carrier transport properties should show a strong magnetic field dependence. Although TPA and exciton dissociation processes were observed here via TPI reactions in TADF-OLEDs, carrier scattering was not observed. Therefore, we infer that carrier scattering is a minor effect in TADF-OLEDs because of the limited change in carrier transport. The latter is due to the aligned levels of highest-occupied and lowest-unoccupied molecular orbitals of the doped emitters relative to those of the host molecules (Supplementary Fig. 4). Doped TADF emitters in the emission layers naturally act as strong carrier traps. Thus, we cannot observe the magnetic response via scattering process

Table 1 Fitting parameters of magneto-electroluminescence under constant current of TADF-OLEDs.

	A_L (−)	B_L (mT)	A_H (−)	B_H (mT)	$\|D\|$ (mT)	$\|E\|$ (mT)
4CzIPN	0.058	5.3	0.11	58.5	40, 46	11
PXZ-TRZ	0.239	6.6	0.18	58.5	49	5.4
ACRXTN	0.091	4.1	0.29	101.0	No data	
2CzPN	0.117	4.8	1.62	81.0	68	15
PIC-TRZ	0.264	5.7	1.83	192.7	98	9.6
3CzTRZ	0.038	4.3	1.87	112.5	No data	

A_L, B_L, A_H, and B_H are the amplitudes and characteristic fields of low-field and high-field effects in magneto-electroluminescence, respectively. $|D|$ and $|E|$ are the absolute values of zero-field splitting parameters (refs. [20, 21]).

because the variation of carrier transport due to the effect of carrier scattering by a triplet exciton can be much smaller than that due to the carrier traps.

Comparison of magnetic field effects under constant current and voltage conditions. To understand the origin of magnetic field effects in OLEDs comprehensively, MEL_J, magneto-resistance, MEL under a constant voltage (MEL_V), and magneto-conductance in 4CzIPN- and 2CzPN-based OLEDs are shown in Fig. 2. In contrast to the positive sign of MEL_J and magneto-resistance (Fig. 2a, c), MEL_V and magneto-conductance include negative components (Fig. 2b, d). Because of the proportionality between electroluminescence intensity and current density, the magneto-efficiency under constant voltage ($M\eta_V$) was calculated by[16]

$$M\eta_V = \mathrm{MEL}_V - \mathrm{MC}\,, \qquad (2)$$

Logarithmic magnetic field effect profiles depicted in Supplementary Fig. 5 separate low-field and high-field effects below and above 0.1 T, respectively.

MEL_Js have positive A_L and A_H, whereas MEL_Vs have both negative A_L and A_H for a 4CzIPN-OLED, and negative and positive A_L and A_H for a 2CzPN-OLED. The $M\eta_V$s have positive A_L and A_H as shown in Fig. 2e. This indicates that negative A_L for MEL_V did not result from decreased emission efficiency, but instead from the decreased current density, i.e., negative signs of magneto-conductance. Furthermore, the magneto-resistance in Fig. 2a, c, and Supplementary Fig. 5a, c can be attributed to TPI-induced triplet dissociation because of the increased net charge carrier density in the emission layers. In a magnetic field, the charge carrier density via exciton dissociation should decrease and the resistance should increase. Although the magneto-resistance profiles had positive A_L and A_H, the magneto-conductance profiles had negative A_L and A_H because of the inverse relationship between resistance and conductance. MEL_J signals in Fig. 2a, c and Supplementary Fig. 5a, c had positive A_H, indicating an increased electroluminescence intensity by the magnetic field, while the positive A_L of MEL_J can be understood as an increase in singlet excitons by the PP mechanism explained above. The high magnetic field suppressed triplet quenching through TPA and triplet dissociation processes as a TPI mechanism, and thus increased the triplet exciton density. It also successively enhanced the upconversion of triplet excitons to singlet states via RISC, resulting in the positive A_H of MEL. In the case of MEL_V signals in Fig. 2b, d and Supplementary Fig. 5b, d, a decrease in current density by the magnetic field results in decreased luminance and a negative A_L. The negative A_H of MEL_V in the 4CzIPN-based device (Fig. 2b and Supplementary Fig. 5b) suggested that there was a larger contribution due to the decreased current density (negative magneto-conductance), relative to suppression of TPA and dissociation processes to increase the electroluminescence intensity. This was because of the small extent of T_1 quenching in the 4CzIPN-based device. Therefore, the low-field and high-field effects result from PP and TPI mechanisms, respectively.

Exciton dynamics in degraded TADF-OLEDs. Magnetic field effects help to understand triplet exciton dynamics in OLEDs. They can also be used to track OLED degradation. Figure 3a, b, and Supplementary Figure 6 plot the decreased luminance and MEL_J profiles of 4CzIPN-, 2CzPN-, and ACRXTN-based OLEDs under a constant current density of 3.0 mA cm^{-2}. L/L_0 is the relative luminance normalized by the initial luminance L_0, which was 1686 cd m^{-2} for 4CzIPN, 492 cd m^{-2} for 2CzPN, and 812 cd m^{-2} for ACRXTN. During the degradation, the MEL_Js monotonically increased with decreased luminance (Fig. 3b), which strongly indicated changes in triplet exciton dynamics during device aging. The discussion below omits the effect of a TTA process on the degradation because it was not the primary channel for triplet quenching under low a current density (3.0 mA cm^{-2}), as shown in Supplementary Figs. 7, 8, and Supplementary Note 1.

The MEL_J signals in the degraded OLEDs were well separated into low-field and high-field effects, and the magnitudes of both (A_L and A_H) were plotted with L/L_0 and operation time in Fig. 3c, d, respectively. The A_Ls and A_Hs exhibited a linear increase with decreased luminance in all devices. The characteristic magnetic fields B_Ls and B_Hs were also plotted with L/L_0 and the operation time in Fig. 3e, f, respectively. The B_Hs of degraded devices were smaller than those of pristine devices that exhibited good agreement with the zero-field splitting values of their excited triplet states, as shown in Table 1. The decreases in B_Hs thus suggest the generation of additional components that alter the magnetic field effect.

One component could be exciplex formation at the interface between the emission layer and hole-blocking layer. This is because of the change in carrier transport in the emission layer during device degradation, which induces a large accumulation of holes and electrons at an interface. This was confirmed by moving the recombination site toward the hole-blocking layer side and observing electromer emission from the SF3-TRZ layer as the hole-blocking layer (Supplementary Fig. 9). The electroluminescence had contributions from an exciplex ($mCBP^{\delta+}$:$SF3\text{-}TRZ^{\delta-}$) (Supplementary Fig. 10a, b), a shoulder emission component over 450–500 nm (Supplementary Fig. 10c), and a red electromer emission in the device with the undoped emission layer containing only mCBP (Fig. 4a). Because the exciplex has high S_1 and T_1 levels of 3.25 and 3.22 eV, respectively (Supplementary Fig. 10a), Förster and Dexter energy-transfer processes to TADF emitters are possible[29]. Exciplex species also generally show magnetic field effects originating from hyperfine interactions or Δg mechanisms (Δg is the difference between the g values of carriers that reside in donor and acceptor molecules)[14]. Figure 4b shows MEL_Js at various emission wavelengths (400–470 nm) of the undoped device that have clear magnetic responses for small (0.1 T) B. The MEL_J signals in Fig. 4b exhibited unusual profiles because they may have included the emission from a monomer, an excimer[30,31], or an electroplex[13,32]. The long-wavelength emission had large amplitudes (Supplementary Fig. 11), even though exciplex species generally show large magnetic responses in emission intensity at short wavelengths because of the distribution of the exciplex activation energy[14]. Although the detailed mechanism and the origin of these results remain unclear, the clear magnetic response of the exciplex under small B strongly suggests that MEL_Js of the degraded devices contain TADF molecule emission via energy transfer from the exciplex

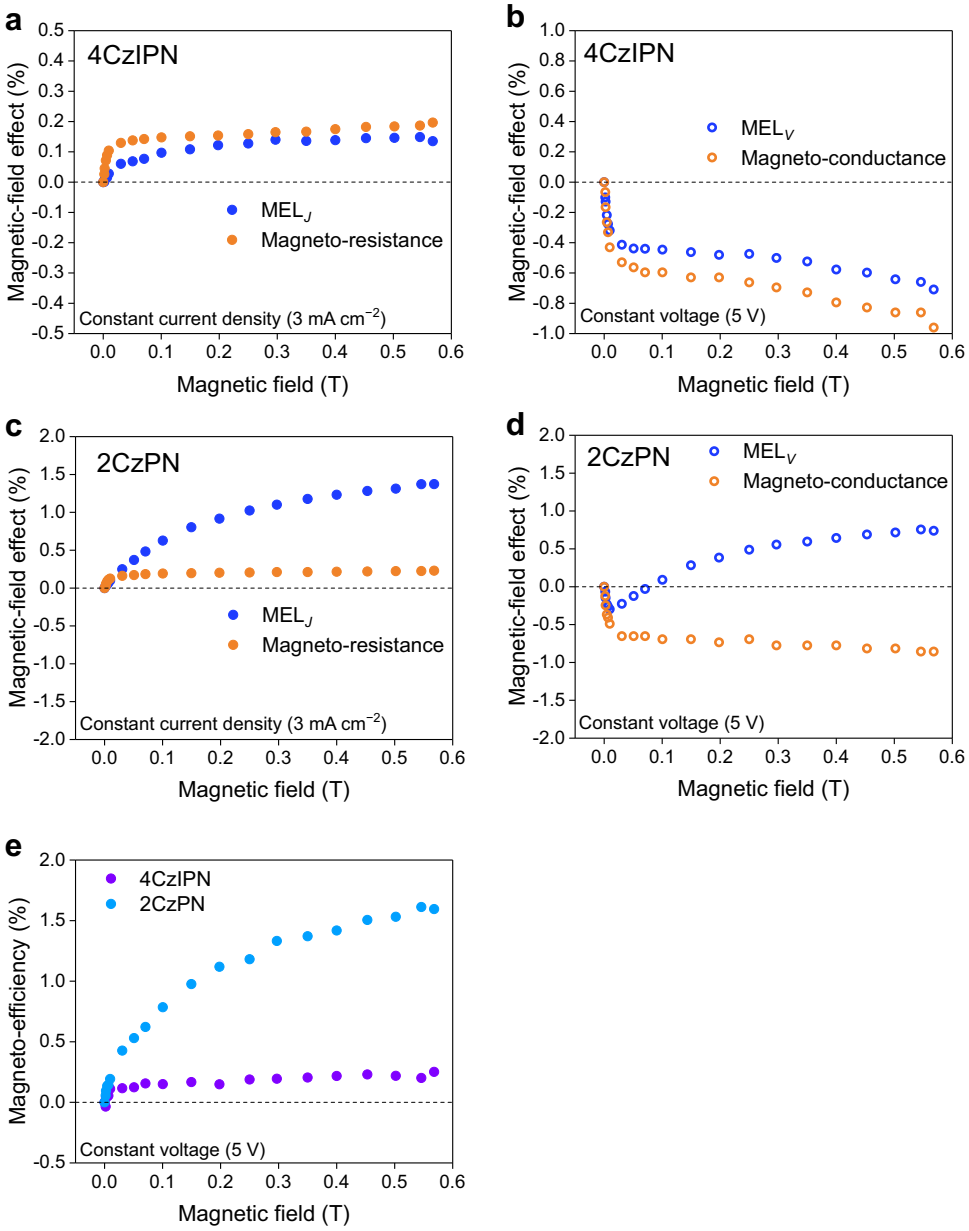

Fig. 2 Magnetic field effects on device characteristics of pristine TADF-OLEDs. a Magnetic responses in device characteristics of 4CzIPN-based OLED under constant current density of 3.0 mA cm^{-2}. **b** Magnetic responses in device characteristics of 4CzIPN-based OLED under constant voltage of 5 V. **c** Magnetic responses in device characteristics of 2CzPN-based OLED under constant current density of 3.0 mA cm^{-2}. **d** Magnetic responses in device characteristics of 2CzPN-based OLED under constant voltage of 5 V. **e** Magneto-efficiencies of 4CzIPN-based and 2CzPN-based OLEDs under constant applied voltage of 5 V.

(mCBP$^{\delta+}$:SF3-TRZ$^{\delta-}$), as shown in Fig. 4c. Thus, we speculate that there were three components of the magnetic field effects in the degraded devices that originated from PP, TPI, and exciplex formation. The interfacial exciplex is an intermediate state that contributes to TADF molecule emission in degraded devices and lowers the B_Hs in device degradation stages, because of the magnetic response of the interfacial exciplex under small B. Although Förster and Dexter energy-transfer processes from the exciplex S_1 and T_1 levels to TADF molecules are possible, Förster energy transfer (FRET) from the film interface should be dominant because of its long-range character. That is, $\eta_{FRET} > \eta_{DEXTER}$, where η_{FRET} and η_{DEXTER} are the B-independent energy transfer efficiencies of Förster and Dexter processes from the exciplex to TADF molecules, respectively. As shown in Fig. 4b, an applied B increases the electroluminescence intensity of the exciplex, indicating an increase in the exciplex S_1 population, $p_{S(exciplex)}$, and a decrease in the population of the exciplex T_1, $p_{T(exciplex)}$. In degraded devices, the increase of $p_{S(exciplex)}$ under B increases the total energy transferred from an exciplex ($\eta_{FRET} \times p_{S(exciplex)} + \eta_{DEXTER} \times p_{T(exciplex)}$) and enhances the TADF emission. That is the increased MEL$_J$ amplitudes of degraded devices.

Electrically generated triplet excitons in the degraded devices significantly suffered from deactivation processes and were quenched because of their long lifetimes. The linear relationships between L/L_0 and A_L indicated that fractions of the triplet excitons, which cannot contribute to electroluminescence, increased with degradation in all devices. These increases were not due to the generation of "static" triplet quenchers, such as decomposed materials, because there was no change in delayed

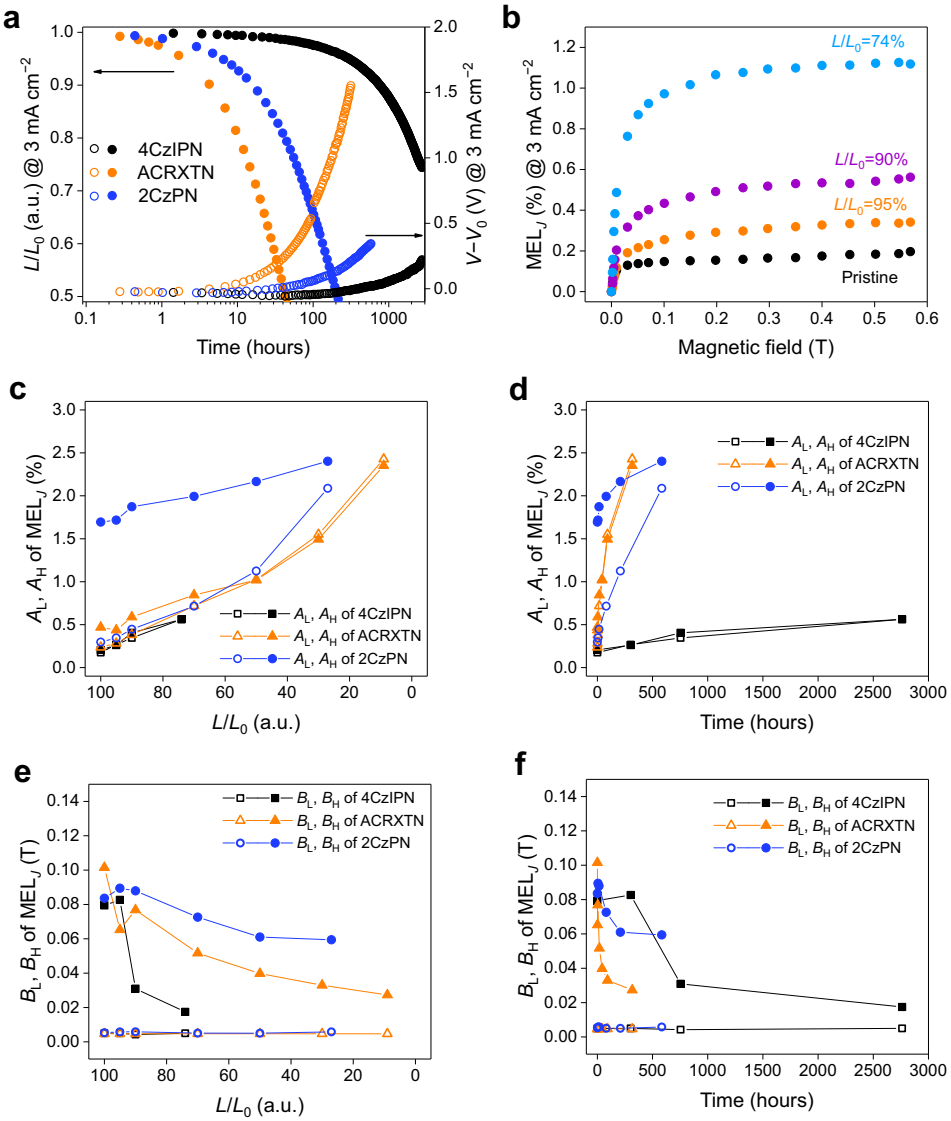

Fig. 3 Tracking TADF-OLED degradation via magnetic field effects. a Luminance decays (L/L_0) and operating voltage ($V - V_0$) characteristics of 4CzIPN-, ACRXTN-, and 2CzPN-based OLEDs with a constant current density of 3.0 mA cm^{-2}. L and V are the luminance and driving voltage, respectively. L_0 and V_0 are the initial luminance and driving voltage of degradation test, respectively. **b** Magneto-electroluminescence (MEL$_J$) profiles of pristine and degraded 4CzIPN-based OLEDs. **c** Relationship between luminance decay and the amplitudes of low-field and high-field effects in MEL$_J$. **d** Relationship between luminance decay and the characteristic fields of low-field and high-field effects in MEL$_J$. **e** Relationship between operating time and the amplitudes of low-field and high-field effects in MEL$_J$. **f** Relationship between operating time and the characteristic fields of low-field and high-field effects in MEL$_J$.

emission lifetime between the pristine and degraded devices (Supplementary Fig. 12) in both transient photoluminescence and electroluminescence decays[33]. We thus estimated the origin for the A_L increases from the aspect of TPI probability. In degraded devices, the PP mechanism converted ^{3}PP into ^{1}PP, and the magnetic field decreased the population of quenched triplet excitons by TPI, resulting in the large A_L. Furthermore, the polarons generated via exciton dissociation of TPI might recombine and generate PPs. Since the generated PPs show the magnetic field effects originating from the PP model again, the increase of polaron density also contributes to gain the A_L.

We conducted displacement current measurements[4] to obtain information on carrier transport and injection in the degraded devices. Displacement current profiles of pristine devices depicted in Supplementary Fig. 13 exhibited increases in capacitance and a plateau at injection voltage (V_{inj}), indicating carrier injection and accumulation. The V_{inj}s depended on doped emitter molecules in the emission layer. The current onset was lower than the 2.6-V threshold voltage (V_{th}) of actual current because the carrier injection and accumulation were originating from surface charges in the emission layer, induced by spontaneous orientation polarization of polar emitter molecules, as reported by Noguchi et al.[4]. The polarization of the doped TADF molecules forms a surface charge δ^- at the interface between the hole-blocking and emission layers, and δ^+ at the interface between the emission layer and hole-blocking layer. The layer-thickness-dependence of the 2CzPN-based OLED in the displacement current profiles (Supplementary Fig. 13d) confirmed that electrons were injected and accumulated in the devices at V_{inj}. In the degraded devices, V_{inj} shifted positive and the accumulation charge densities were reduced because they were proportional to the difference between V_{inj} and V_{th}. This indicated the formation of the charge carrier traps, especially electron traps in the emission layer, and simultaneously suppressed carrier injection[4]. Hence, the generation of carrier traps in degraded devices changed the charge transport properties and increased exciton quenching by TPI. As

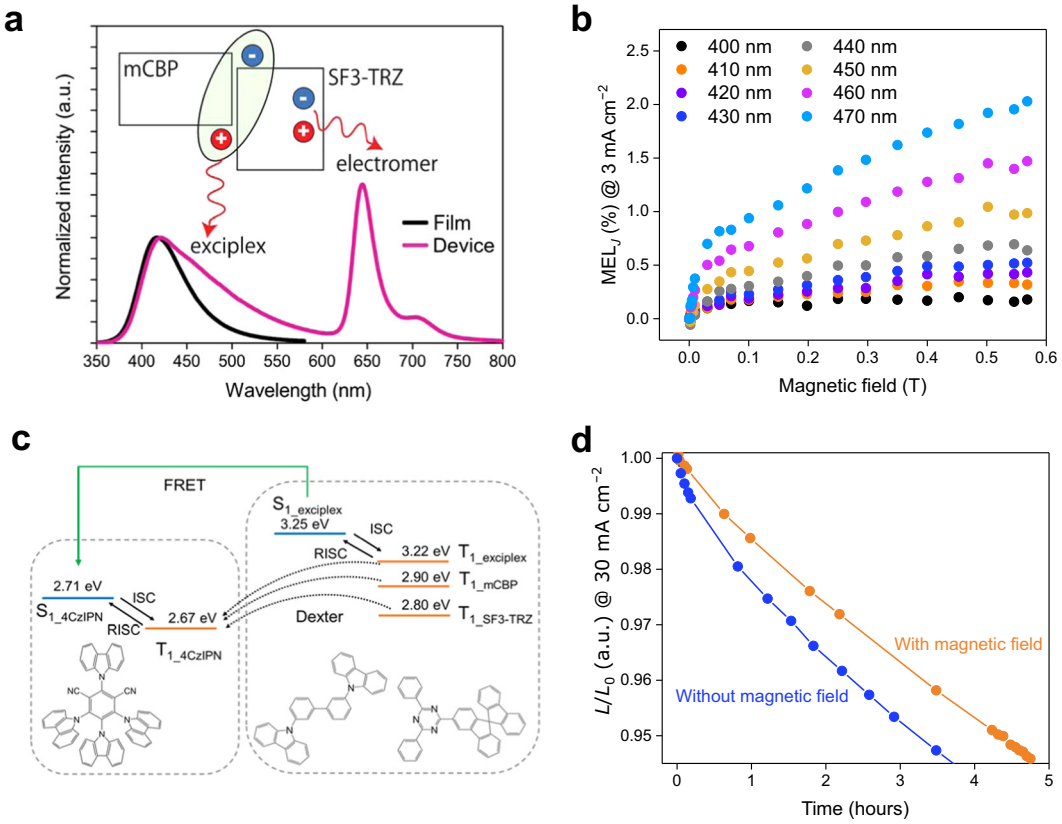

Fig. 4 Origin of the degradation event in TADF-OLEDs. a Photoluminescence spectrum of the co-deposited film of 50 wt%-mCBP:SF3-TRZ, and electroluminescence spectrum of the device based on the undoped emission layer (only mCBP). **b** Magneto-electroluminescence profiles of the device based on the undoped emission layer with various emission wavelengths. **c** Schematic of energy transfer to TADF emitters in degraded devices. **d** Luminance decay curves of 4CzIPN-based OLEDs under constant high current of 30 mA cm^{-2}. The pixels were fabricated on same substrate at the same time.

reported previously, undesired triplet reactions such as TPI are origins of carrier trap formation in TADF-OLEDs[9,34,35].

A_Hs for degraded devices include the effects of TPI and exciplex formation. The increase in A_Hs also suggested, as explained above, an increase in the fraction of triplet exciton quenching via TPI and nonradiative exciplex formation at the emission layer/hole-blocking layer interface. We understand device degradation by observing magnetic field effects, including PP and TPI mechanisms and exciplex formation.

Furthermore, the linear relationships between L/L_0s and the MEL$_J$ amplitudes for pristine and degraded devices originated from both changes in electroluminescence intensity under a magnetic field ($\Delta I_{EL}(B)$) and that without a magnetic field ($I_{EL}(0)$). The relative $\Delta I_{EL}(B)$s increase during initial device degradation, and decrease during the latter part (see Supplementary Fig. 14 and Supplementary Note 2). The magnetic responses of TPI and exciplex formation increase the magnitudes of MEL$_J$s. However, the recovery of emission intensity, i.e., $\Delta I_{EL}(B)$s, decreases in extremely inefficient devices because the conversion of ^{3}PP to ^{1}PP, and the suppression of TPI, cannot contribute to the emission of the TADF emitters in degraded devices. An example would be an extremely biased condition.

Supplementary Figure 15 shows the relationship between electroluminescence quantum efficiencies and MEL$_J$ profiles under several current densities of pristine and degraded 4CzIPN-based devices. The quantum efficiencies of degraded devices under low current density exhibited significant decreases relative to those under high current density (Supplementary Fig. 15d). Similarly, MEL$_J$s of the degraded devices under the low current density of 0.1 mA cm^{-2} had more substantial changes, indicating a large increase in deactivation of triplet excitons (Supplementary Fig. 15a, b). In the degraded devices, holes are transported to the emission layer/hole-blocking layer interface and become excess carriers, resulting in TPI[36] and exciplex formation at the interface because of suppressed electron injection. Thus, quantum efficiencies decreased during degradation. Under 3.0 and 10 mA cm^{-2} current densities, quantum efficiencies were enhanced and MEL$_J$s decreased, because electron injection into the emission layer increased. Under 100 mA cm^{-2} current density, MEL$_J$s of the pristine and degraded devices increased again, in the same manner, indicating an increase in the fraction of triplet exciton quenching via TPI and nonradiative exciplex formation.

Device operation under external magnetic fields should lengthen the operational lifetime because the field reduces the triplet density and suppresses undesired TPI. Figure 4d shows the luminance decay curves with and without a 0.2-T magnetic field under 30 mA cm^{-2} current density. The field slightly but clearly improved the device stability. Specifically, the averaged LT$_{95}$ (which is the time at which the luminance decreases to 95% of initial luminance) was 3.3 h without and 4.0 h with the magnetic field. Here, we assume that

$$\mathrm{LT} \times L_0^n = \text{const.} \quad (3)$$

where n is an acceleration factor[37]. In Supplementary Table 1, we obtain $n = 2.0$, and LT$_{95}$ is predicted to be 369 h under 3.0 mA cm^{-2} current density and a 0.2-T magnetic field. This is a 20% improvement in device stability and strongly indicates that either

or both the decrease in triplet excitons and the suppression of TPI can enhance device stability. That is because the field reduces the triplet exciton density under low fields (PP model) and suppresses undesired TPI at high fields.

In conclusion, we investigated the magnetic field effects on the characteristics of TADF-OLEDs to understand the underlying dynamics of triplet excitons during electrical excitation and during OLED degradation. The results indicate that the increase in TPI is the main reason for decreased luminance in OLED degradation. Furthermore, from changes in high-field effects of degraded devices, we confirmed that undesired exciton generation, such as interfacial exciplex formation, also reduces the electroluminescence quantum yield. The analysis based on magnetic field effects can thus nondestructively clarify the dynamics of triplet excitons in devices under operation.

Methods

Materials. Various TADF molecules were used as emitters in OLEDs, and all were synthesized here (Fig. 1a). The 4CzIPN, PXZ-TRZ, and ACRXTN molecules have short exciton lifetimes relative to those of 2CzPN, PIC-TRZ, and 3CzTRZ. 4CzIPN, PXZ-TRZ, ACRXTN, 2CzPN, PIC-TRZ, and 3CzTRZ are 1,2,3,5-tetrakis(carbazol-9-yl)-4,6-dicyanobenzene, 10-[4-(4,6-diphenyl-1,3,5-triazin-2-yl)phenyl]-10H-phenoxazine, 3-(9,9-dimethylacridin-10(9H)-yl)-9H-xanthen-9-one, 1,2-bis(carbazol-9-yl)-4,5-dicyanobenzene, 2-biphenyl-4,6-bis(12-phenylin-dolo[2,3-a]carbazol-11-yl)-1,3,5-triazine, and 9-(3-(9H-carbazol-9-yl)-9-(4-(4,6-diphenyl-1,3,5-triazin-2-yl)phenyl)-9H-carbazol-6-yl)-9H-carbazole, respectively.

Device fabrication. The OLEDs were fabricated via vacuum vapor deposition without exposure to ambient air. The device structure (Supplementary Fig. 1) is ITO (100 nm)/HAT-CN (10 nm)/Tris-PCz (30 nm)/mCBP or mCP (5 nm)/emission layer (30 nm)/SF3-TRZ (10 nm)/30 wt% Liq:SF3-TRZ (50 nm)/Liq (2 nm)/Al (100 nm). The emission layers were formed using a co-deposition technique. For 3CzTRZ, mCP was adopted as a host and an electron-blocking layer because of triplet exciton confinement. In other cases, mCBP was used as a host and an electron-blocking layer. ITO, HAT-CN, Tris-PCz, mCBP, mCP, SF3-TRZ, and Liq are indium tin oxide, 1,4,5,8,9,11-hexaazatriohenyleane hexacarbonitrile, 9,9′-diphenyl-6-(9-phenyl-9H-carbazol-3-yl)-9H,9′H-3,3′-bicarbazole, 3,3′-di(9*H*-carbazol-9-yl)-1,1′-biphenyl, 1,3-bis(N-carbazolyl)benzene, 2-(9,9′-spirobi[fluoren]-3-yl)-4,6-diphenyl-1,3,5-triazine and 8-hydroxyquinolinolato-lithium, respectively. All organic layers, except for the Liq layer, were deposited at a rate of 0.1 nm/s, while the Liq layer was deposited at 0.03 nm/s. The deposition rates of Al were 0.1 nm/s. The device area was approximately 0.04 cm^2. After fabrication, the devices were immediately encapsulated under glass using epoxy glue in a nitrogen-filled glovebox ($H_2O > 0.1$ ppm, $O_2 > 0.1$ ppm).

Sample characterization. Electroluminescence quantum efficiency measurements were performed using a calibrated luminance meter (CS-2000, Konica Minolta). For the device lifetime tests, the luminance and spectra of the driving devices in the normal direction were measured using a luminance meter (SR-3AR, TOPCON) under constant current density driving conditions. For the displacement current measurement, repeated-triangular voltage signals were applied to each device using a function generator (WaveStation 2052, Teledyne Lecroy) and the displacement current was amplified using a current amplifier (CA5350, NF). The applied voltage and the amplified current were measured using an oscilloscope (HDO4054A, Teledyne Lecroy). The applied voltage signal ranged from −4 to 4 V and the scan rate was 100 V s^{-1}. For the transient electroluminescence measurements, pulsed voltages were applied using a function generator. The emitted light was detected with a photomultiplier tube module (H10721-01, Hamamatsu Photonics) and the signals were amplified with a current amplifier (DHPCA-100, Femto). All signals were collected using an oscilloscope with signal averaging performed over 1000 measurements. Photoluminescence quantum yields were measured using the Quantaurus-QY system (C11347-11, Hamamatsu Photonics) in flowing argon gas at 340-nm excitation. Transient photoluminescence decay profiles were recorded with a Quantaurus-Tau system (C11367-03, Hamamatsu Photonics) in ambient air. Fluorescence and phosphorescence spectra were acquired with a FP8600 (JASCO) at room temperature and 77 K, respectively.

Characterization of magnetic field effects. In magnetic field effect measurements, the magnetic field was applied along the direction of the substrate, and the magnitude (B) was varied over 0–0.57 T. Electroluminescence spectra were collected with a fiber spectrometer (MAYA2000PRO, Ocean) and the driving voltage (V) or current density (J) at each magnitude of the magnetic field was determined with a source-measure unit (Keithley 2612B, Tektronix). Measurements were performed for two cycles from 0 to 0.57 T and from 0.57 to 0 T, and were averaged into one cycle. Magneto-electroluminescence (MEL_J) and magneto-resistance under constant current conditions were calculated from

$$\mathrm{MEL}_J = \frac{I_{EL}(B) - I_{EL}(0)}{I_{EL}(0)}, \tag{4}$$

$$\mathrm{magneto-resistance} = \frac{V(B) - V(0)}{V(0)}. \tag{5}$$

Magneto-electroluminescence (MEL_V) and magneto-conductance under constant voltage conditions were calculated from

$$\mathrm{MEL}_V = \frac{I_{EL}(B) - I_{EL}(0)}{I_{EL}(0)}, \tag{6}$$

$$\mathrm{magneto-conductance} = \frac{J(B) - J(0)}{J(0)}, \tag{7}$$

where $I_{EL}(B)$, $V(B)$, and $J(B)$ were the electroluminescence intensity, the voltage, and the current density under magnetic field B, respectively. The fitting analysis of magnetic responses to separate low-field and high-field effects were performed with Lorentzian and non-Lorentzian functions with four parameters for amplitudes and characteristic magnetic fields. All the parameters were constrained as positive values in the fits. Initial values of A_L, A_H, B_L, and B_H were 0.05, 0.1, 3, and 10 mT, respectively.

Data availability

The data that support the findings of this study are available from the corresponding author upon request.

Received: 20 November 2019; Accepted: 13 March 2020;
Published online: 24 April 2020

References

1. Kondakov, D. Y., Lenhart, W. C. & Nichols, W. F. Operational degradation of organic light-emitting diodes: mechanism and identification of chemical products. *J. Appl. Phys.* **101**, 024512 (2007).
2. Kondakov, D. Y. Role of chemical reactions of arylamine hole transport materials in operational degradation of organic light-emitting diodes. *J. Appl. Phys.* **104**, 084520 (2008).
3. Scholz, S., Kondakov, D. Y., Lüssem, B. & Leo, K. Degradation mechanisms and reactions in organic light-emitting devices. *Chem. Rev.* **115**, 8449–8503 (2015).
4. Noguchi, Y. et al. Charge carrier dynamics and degradation phenomena in organic light-emitting diodes doped by a thermally activated delayed fluorescence emitter. *Org. Electron.* **17**, 184–191 (2015).
5. Giebink, N. C., D'Andrade, B. W., Weaver, M. S., Brown, J. J. & Forrest, S. R. Direct evidence for degradation of polaron excited states in organic light emitting diodes. *J. Appl. Phys.* **105**, 124514 (2009).
6. Lee, J. et al. Hot excited state management for long-lived blue phosphorescent organic light-emitting diodes. *Nat. Commun.* **8**, 15566 (2017).
7. Song, W. & Lee, J. Y. Degradation mechanism and lifetime improvement strategy for blue phosphorescent organic light-emitting diodes. *Adv. Opt. Mater.* **5**, 1600901 (2017).
8. Baldo, M. A., Adachi, C. & Forrest, S. R. Transient analysis of organic electrophosphorescence. II. Transient analysis of triplet-triplet annihilation. *Phys. Rev. B* **62**, 10967 (2000).
9. Tanaka, M., Noda, H., Nakanotani, H. & Adachi, C. Effect of carrier balance on device degradation of organic light-emitting diodes based on thermally activated delayed fluorescence emitters. *Adv. Electron. Mater.* **5**, 1800708 (2019).
10. Kalinowski, J., Cocchi, M., Virgili, D., Di Marco, P. & Fattori, V. Magnetic field effects on emission and current in Alq3-based electroluminescent diodes. *Chem. Phys. Lett.* **380**, 710–715 (2003).
11. Peng, Q., Li, X. & Li, F. Time-resolved spin-dependent processes in magnetic field effects in organic semiconductors. *J. Appl. Phys.* **112**, 114512 (2012).
12. Zhou, J. et al. Charge-transfer-featured materials—promising hosts for fabrication of efficient OLEDs through triplet harvesting via triplet fusion. *Chem. Commun.* **50**, 7586–7589 (2014).
13. Kalinowski, J., Cocchi, M., Virgili, D., Fattori, V. & Di Marco, P. Magnetic field effects on organic electrophosphorescence. *Phys. Rev. B* **70**, 205303 (2004).
14. Lei, Y. et al. Ultralarge magneto-electroluminescence in exciplex-based devices driven by field-induced reverse intersystem crossing. *Adv. Opt. Mater.* **4**, 694–699 (2016).

15. Deng, J. et al. Guest concentration, bias current, and temperature-dependent sign inversion of magneto-electroluminescence in thermally activated delayed fluorescence devices. *Sci. Rep.* **7**, 44396 (2017).
16. Pan, R. et al. Extraordinary magnetic field effects mediated by spin-pair interaction and electron mobility in thermally activated delayed fluorescence-based OLEDs with quantum-well structure. *J. Mater. Chem. C* **7**, 2329–2421 (2019).
17. Prigodin, V. N., Bergeson, J. D., Lincoln, D. M. & Epstein, A. J. Anomalous room temperature magnetoresistance in organic semiconductors. *Synth. Met.* **156**, 757–761 (2006).
18. Keevers, T. L., Baker, W. J. & McCamey, D. R. Theory of exciton-polaron complexes in pulsed electrically detected magnetic resonance. *Phys. Rev. B* **91**, 205206 (2015).
19. Devir-Wolfman, A. H. et al. Short-lived charge-transfer excitons in organic photovoltaic cells studied by high-field magneto-photocurrent. *Nat. Commun.* **5**, 4529 (2014).
20. Ogiwara, T., Wakikawa, Y. & Ikoma, T. Mechanism of intersystem crossing of thermally activated delayed fluorescence molecules. *J. Phys. Chem. A* **119**, 3415–3418 (2015).
21. Evans, E. W. et al. Vibrationally assisted intersystem crossing in benchmark thermally activated delayed fluorescence molecules. *J. Phys. Chem. Lett.* **9**, 4053–4058 (2018).
22. Kondakov, D. Y., Pawlik, T. D., Hatwar, T. K. & Spindler, J. P. Triplet annihilation exceeding spin statistical limit in highly efficient fluorescent organic light-emitting diodes. *J. Appl. Phys.* **106**, 124510 (2009).
23. Song, D., Zhao, S., Luo, Y. & Aziz, H. Causes of efficiency roll-off in phosphorescent organic light emitting devices: triplet-triplet annihilation versus triplet-polaron quenching. *Appl. Phys. Lett.* **97**, 243304 (2010).
24. Inoue, M. et al. Effect of reverse intersystem crossing rate to suppress efficiency roll-off in organic light-emitting diodes with thermally activated delayed fluorescence emitters. *Chem. Phys. Lett.* **644**, 62–67 (2016).
25. Kim, A. et al. Degradation of blue-phosphorescent organic light-emitting devices involves exciton-induced generation of polaron pair within emitting layers. *Nat. Commun.* **9**, 1211 (2018).
26. Cox, M., Janssen, P., Zhu, F. & Koopmans, B. Traps and trions as origin of magnetoresistance in organic semiconductors. *Phys. Rev. B* **88**, 035202 (2013).
27. Ern, V. & Merrifield, R. E. Magnetic field effect on triplet exciton quenching in organic crystals. *Phys. Rev. Lett.* **21**, 609 (1968).
28. Wittmer, M. & Zschokke-Gränacher, I. Exciton–charge carrier interactions in the electroluminescence of crystalline anthracene. *J. Chem. Phys.* **63**, 4187 (1975).
29. Uoyama, H. Highly efficient organic light-emitting diodes from delayed fluorescence. *Nature* **492**, 234–238 (2012).
30. Hoffman, S. T. et al. Triplet excimer emission in a series of 4,4′-Bis(N-carbazolyl)-2,2′-biphenyl derivatives. *J. Phys. Chem. B* **115**, 414–421 (2011).
31. Bagnich, S. A. et al. Excimer formation by steric twisting in carbazole and triphenylamine-based host materials. *J. Phys. Chem. C* **119**, 2380–2387 (2015).
32. Granlund, T., Pettersson, L. A. A., Anderson, M. R. & Inganäs, O. Interference phenomenon determines the color in an organic light emitting diode. *J. Appl. Phys.* **81**, 8097 (1997).
33. Schmidt, T. D., Jäger, L., Noguchi, Y., Ishii, H. & Brütting, W. Analyzing degradation effects of organic light-emitting diodes via transient optical and electrical measurements. *J. Appl. Phys.* **117**, 215502 (2015).
34. Song, W., Kim, T., Lee, J. Y., Lee, Y. & Jeong, H. Investigation of degradation mechanism of phosphorescent and thermally activated delayed fluorescent organic light-emitting diodes through doping concentration dependence of lifetime. *J. Ind. Eng. Chem.* **68**, 350–354 (2018).
35. Sohn, J. et al. Degradation mechanism of blue thermally activated delayed fluorescent organic light-emitting diodes under electrical stress. *Org. Electron.* **70**, 286–291 (2019).
36. Sandanayaka, A. S. D., Yoshida, K., Matsushima, T. & Adachi, C. Exciton quenching behavior of thermally activated delayed fluorescence molecules by charge carriers. *J. Phys. Chem. C* **119**, 7631–7636 (2015).
37. Féry., C., Racine, B., Vaufrey, D., Doyeux, H. & Cinà, S. Physical mechanism responsible for the stretched exponential decay behavior of aging organic light-emitting diodes. *Appl. Phys. Lett.* **87**, 213502 (2005).

Acknowledgements

This work was supported financially by the Program for Building Regional Innovation Ecosystems of the Ministry of Education, Culture, Sports, Science and Technology (MEXT), Japan. The authors thank Ms. Keiko Kusuhara and Ms. Nozomi Nakamura of Kyushu University for providing chemicals for the OLEDs, and Dr. Kenichi Goushi and Dr. Yoichi Tsuchiya of Kyushu University for helpful discussions. The authors also acknowledge Dr. Hiroshi Fujimoto, Dr. Hin-Wai Mo, and Ms. Kaori Nagayoshi from i^3-opera for their helps in OLED fabrication.

Author contributions

The project was conceived and designed by M.T. M.T. prepared the samples and measured their properties. M.T., H.N., and R.N. analyzed all the data. C.A. supervised the project. All authors contributed to writing the paper and critically commented on the project.

Competing interests

The authors declare no competing interests.

Additional information

Supplementary information is available for this paper at https://doi.org/10.1038/s43246-020-0019-0.

Correspondence and requests for materials should be addressed to H.N. or C.A.

Reprints and permission information is available at http://www.nature.com/reprints

Publisher's note Springer Nature remains neutral with regard to jurisdictional claims in published maps and institutional affiliations.